Stop pair production at the LHC with aMC@NLO
Validation figures

**C. Degrande, B. Fuks, V. Hirschi,
J. Proudom & H.S. Shao**

November 3, 2014

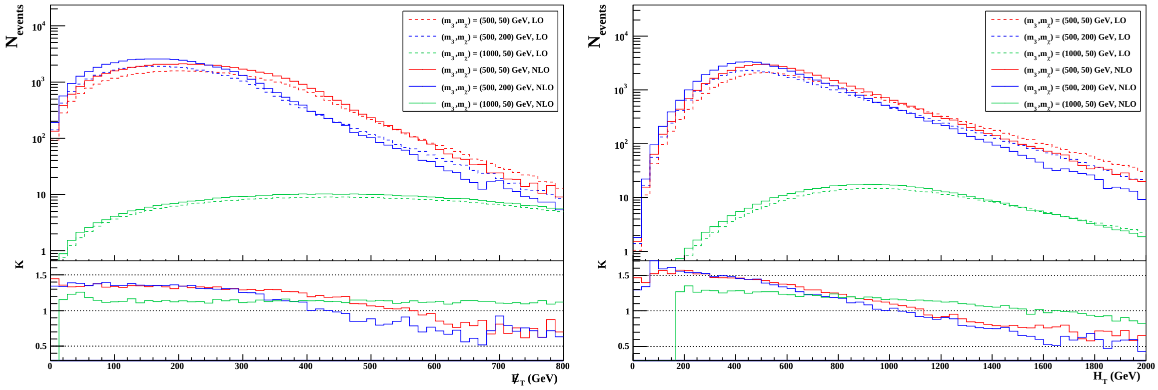

Figure 1: Global event variables: the missing transverse energy distribution (left) and the hadronic activity (right).

1 Simulation setup

Parton-level events have been simulated with the MadGraph5_aMC@NLO program [1], using the UFO module [2] generated by making use of FeynRules [3] and NloCT [4]. Hard scattering elements have been generated from the interactions embedded in the Lagrangian

$$\mathcal{L}_3 = D_\mu \sigma_3^\dagger D^\mu \sigma_3 - m_3^2 \sigma_3^\dagger \sigma_3 + \frac{i}{2} \bar\chi \partial\!\!\!/ \chi - \frac{1}{2} m_\chi \bar\chi \chi + \Big[\sigma_3 \bar t \big(\tilde g_L P_L + \tilde g_R P_R \big) \chi + \text{h.c.} \Big] ,$$

as indicated in Ref. [5] where more information can be found. We recall that this Lagrangian describes the dynamics of a stop field σ_3 of mass m_3 that is allowed to decay into a Majorana gauge-singlet fermion χ (of mass m_χ) and a top quark t. The numerical results presented in this document are based on benchmark scenarios where the $\tilde g_{L,R}$ parameters are fixed to values typical of supersymmetric models featuring a bino-like neutralino and a maximally-mixing top squark,

$$\tilde g_L = 0.25 \qquad \text{and} \qquad \tilde g_R = 0.06 \ .$$

We consider three benchmark points for which the stop and neutralino masses are fixed to $(m_3, m_\chi) = (500, 50)$ GeV, $(1000, 50)$ GeV and $(500, 200)$ GeV, respectively. For each scenario, we have generated 10^6 events at the leading order accuracy and the same number at the next-to-leading order one.

The decay of the stop has been performed by using the MadSpin [6] package, and parton-level events generated in this way have then be showered and hadronized as implemented in the Pythia 8.1 program [7]. Hadronized events have then been processed with an anti-k_T algorithm with a radius parameter set to $R = 0.4$ [8], as implemented in the FastJet program [9].

From all the reconstructed jets, only those with a transverse-momentum $p_T > 20$ GeV and a pseudrapidity $|\eta| < 2.5$ have been retained. In our analysis, we have also only considered leptons with $p_T > 10$ GeV and $|\eta| < 2.5$. Moreover, we have removed all leptons lying at an angular distance $\Delta R < 0.4$ of any selected jet. All the differential distributions presented here have been generated with MadAnalysis 5 [10], the normalization being fixed to an integrated luminosity of 100 fb^{-1}. In each figure, we indicate both the leading-order and next-to-leading results, as well as their ratio called K-factor (which is differential here).

2 Global event variables

We present in Figure 1 the missing energy distribution (left) and the total transverse hadronic activity (right) that are calculated as

$$H_T = \sum_{\text{hadronic particles}} |\vec p_T| \qquad \text{and} \qquad \not\!\!E_T = \Big| - \sum_{\text{visible particles}} \vec p_T \Big| ,$$

where the sum are performed over all the event particles.

3 Zero lepton analysis

From the inclusively generated event sample, we select events which do not feature any final state electron or muon. We present in Figure 2 various distributions illustrating the properties of the two leading jets.

4 Single lepton analysis

From the inclusively generated event sample, we select events which feature exactly one final state electron or muon. We present in Figure 3 and Figure 4 various distributions illustrating the properties of the lepton and of the leading jets.

5 Dilepton analysis

From the inclusively generated event sample, we select events which feature exactly two final state electrons or muons. We present in Figure 5, Figure 6 and Figure 7 various distributions illustrating the properties of the leptons and of the two leading jets.

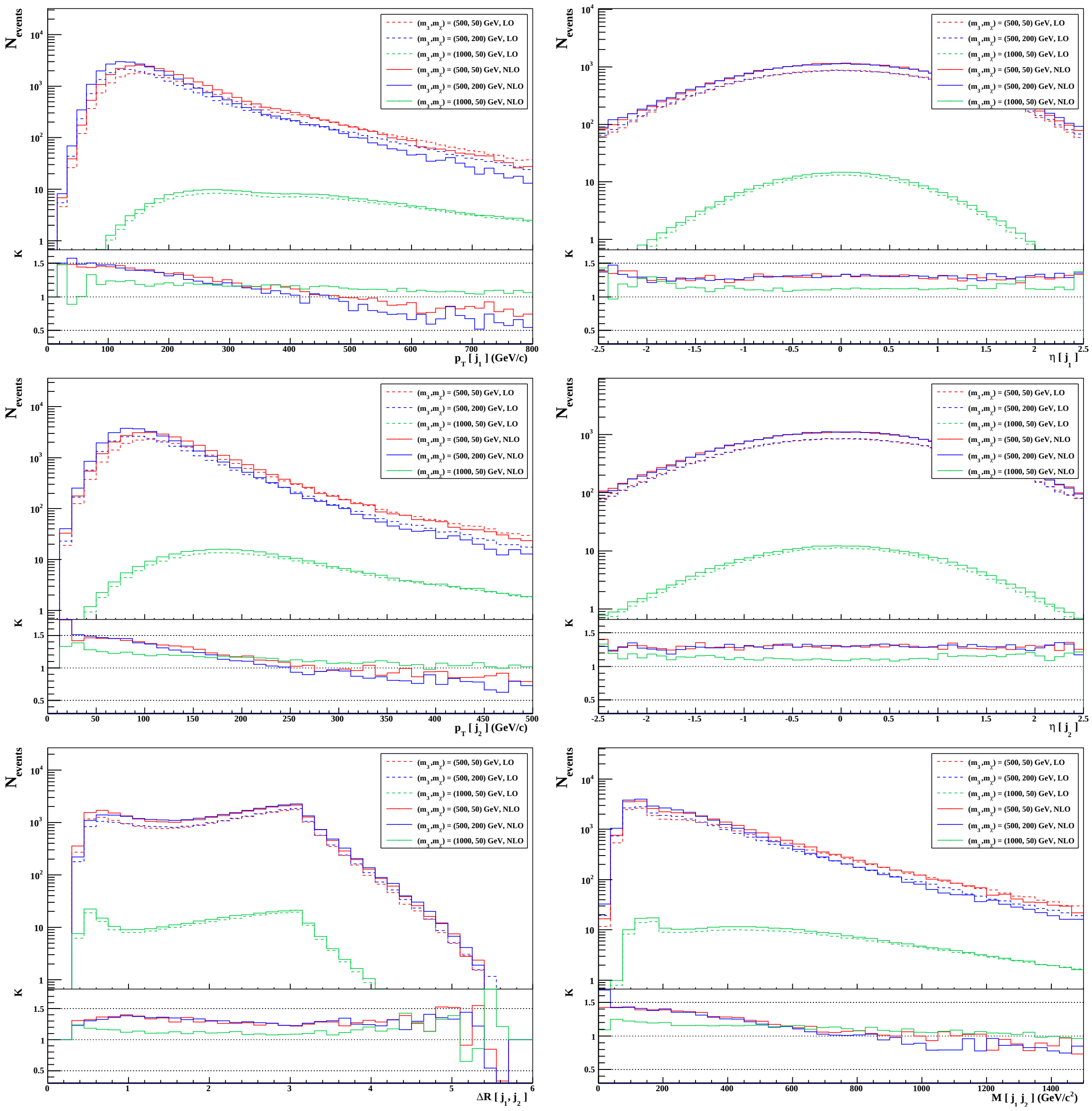

Figure 2: Zero lepton signal region: jet properties.

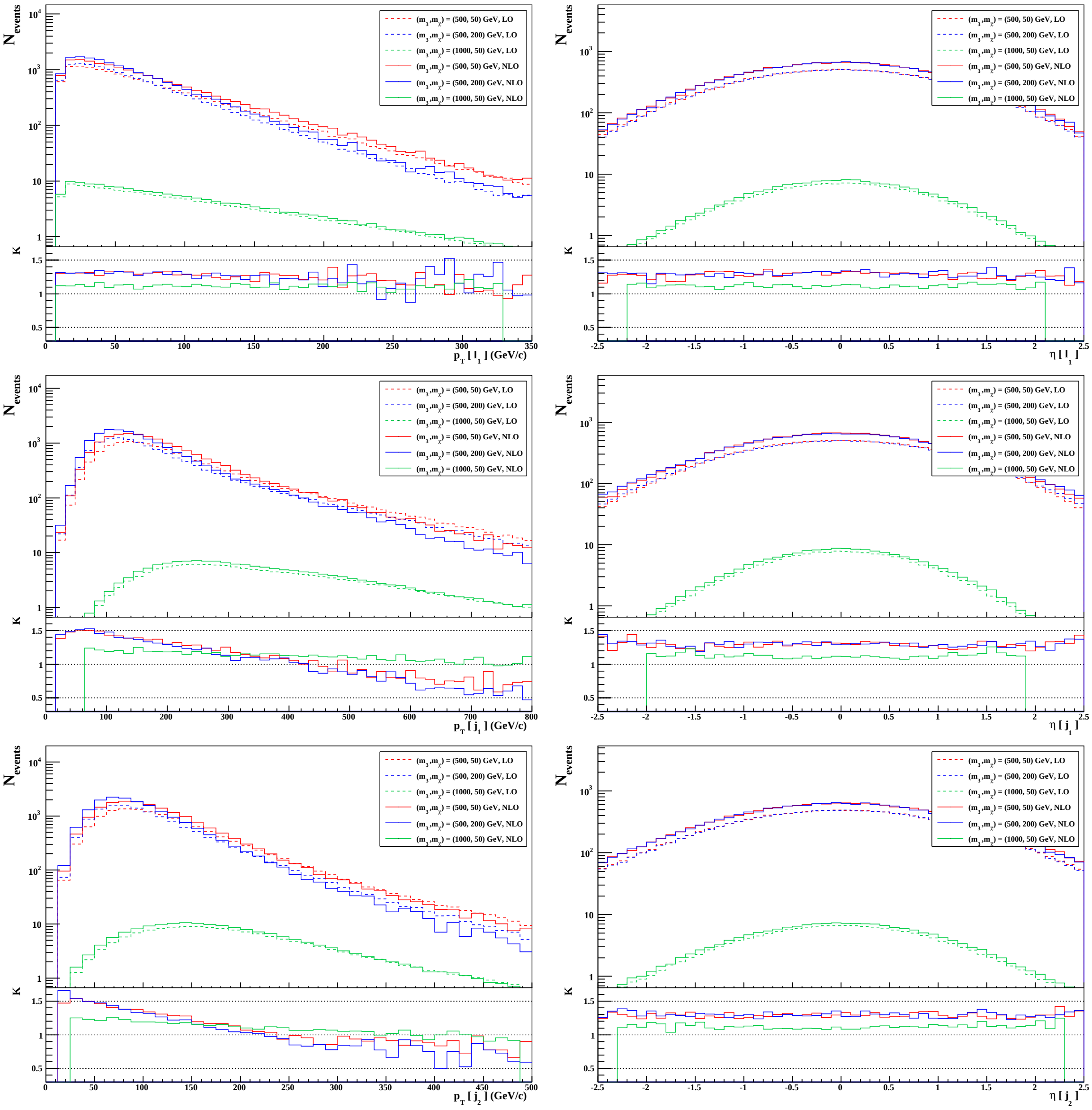

Figure 3: Single lepton signal region: lepton and jet properties.

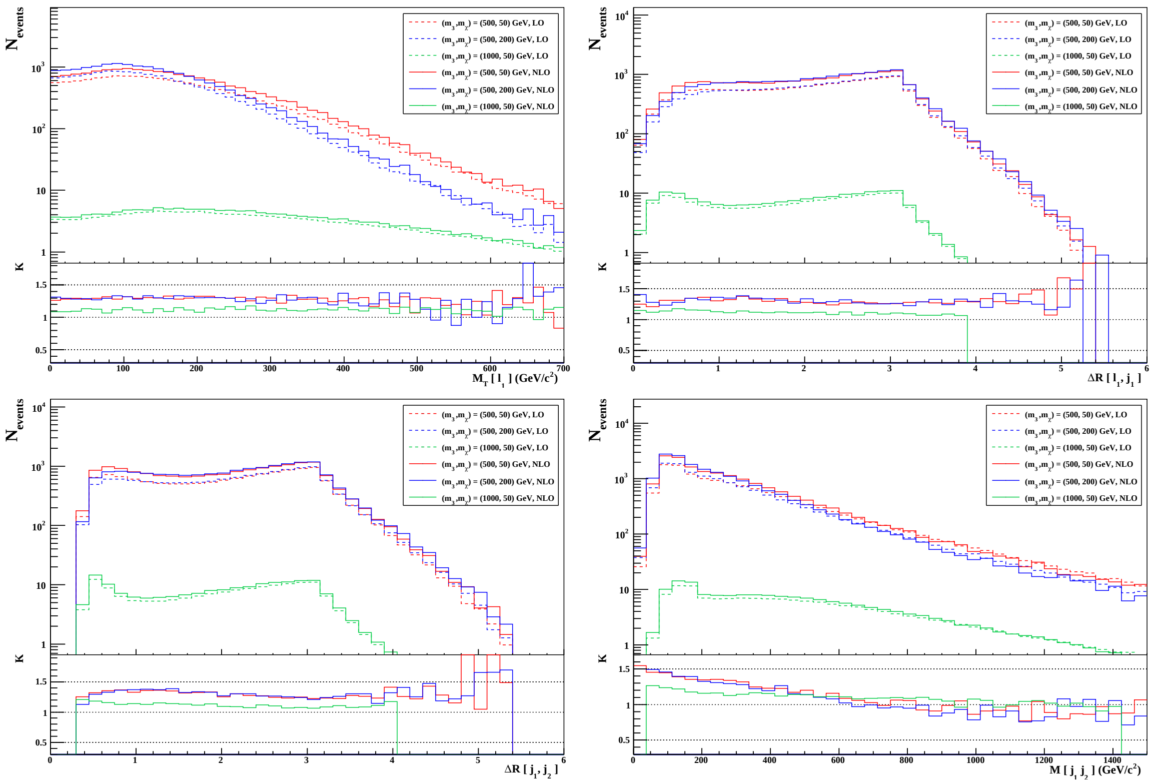

Figure 4: Single lepton signal region: lepton and jet properties (continued).

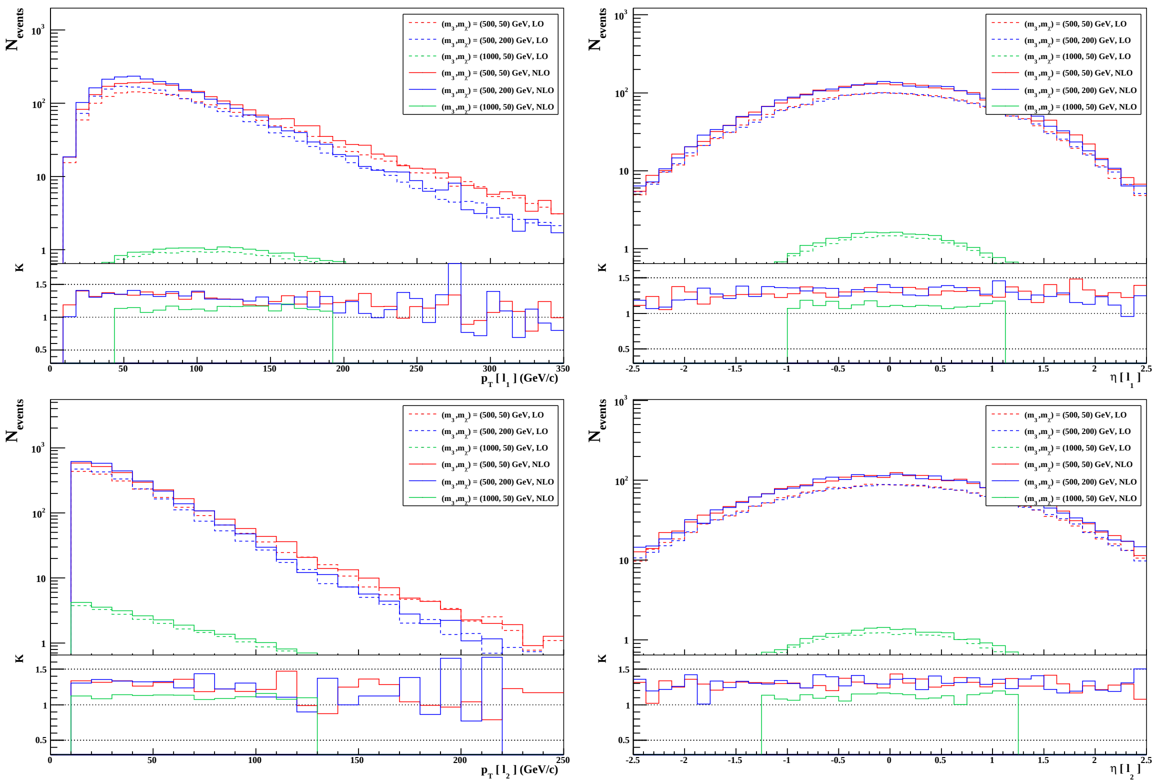

Figure 5: Dilepton signal region: lepton properties.

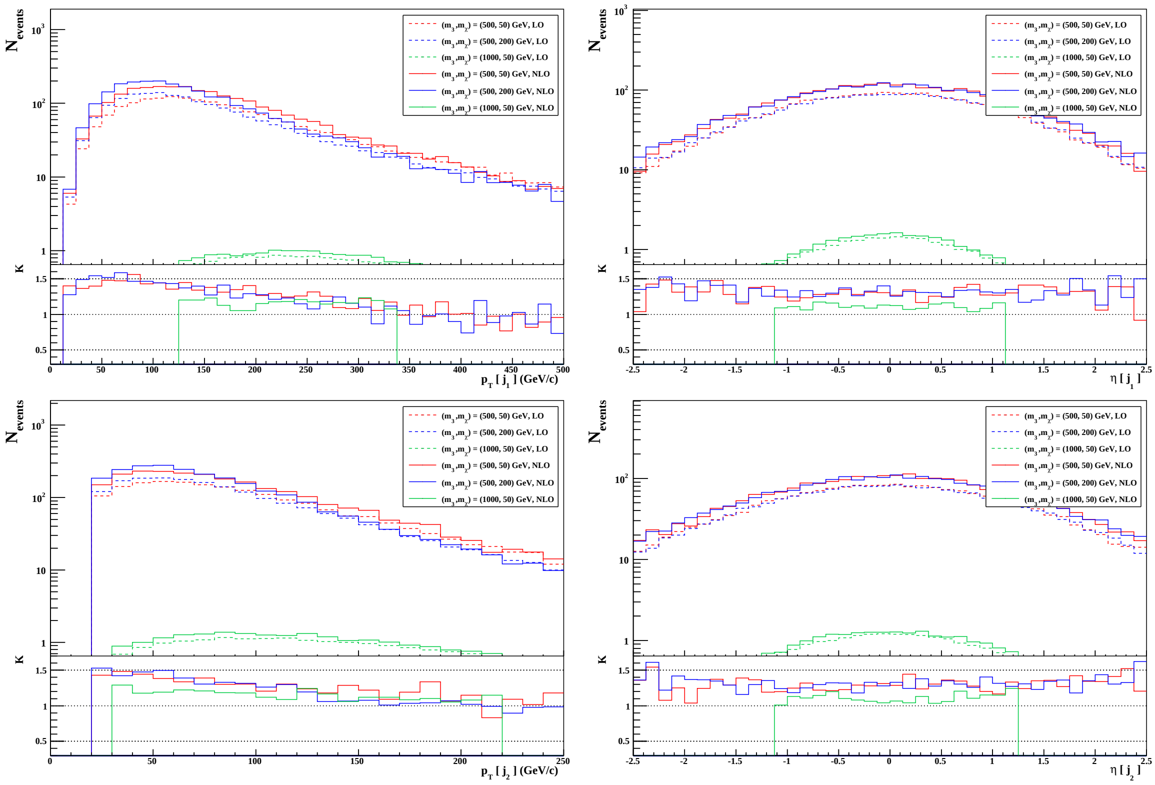

Figure 6: Dilepton signal region: jet properties.

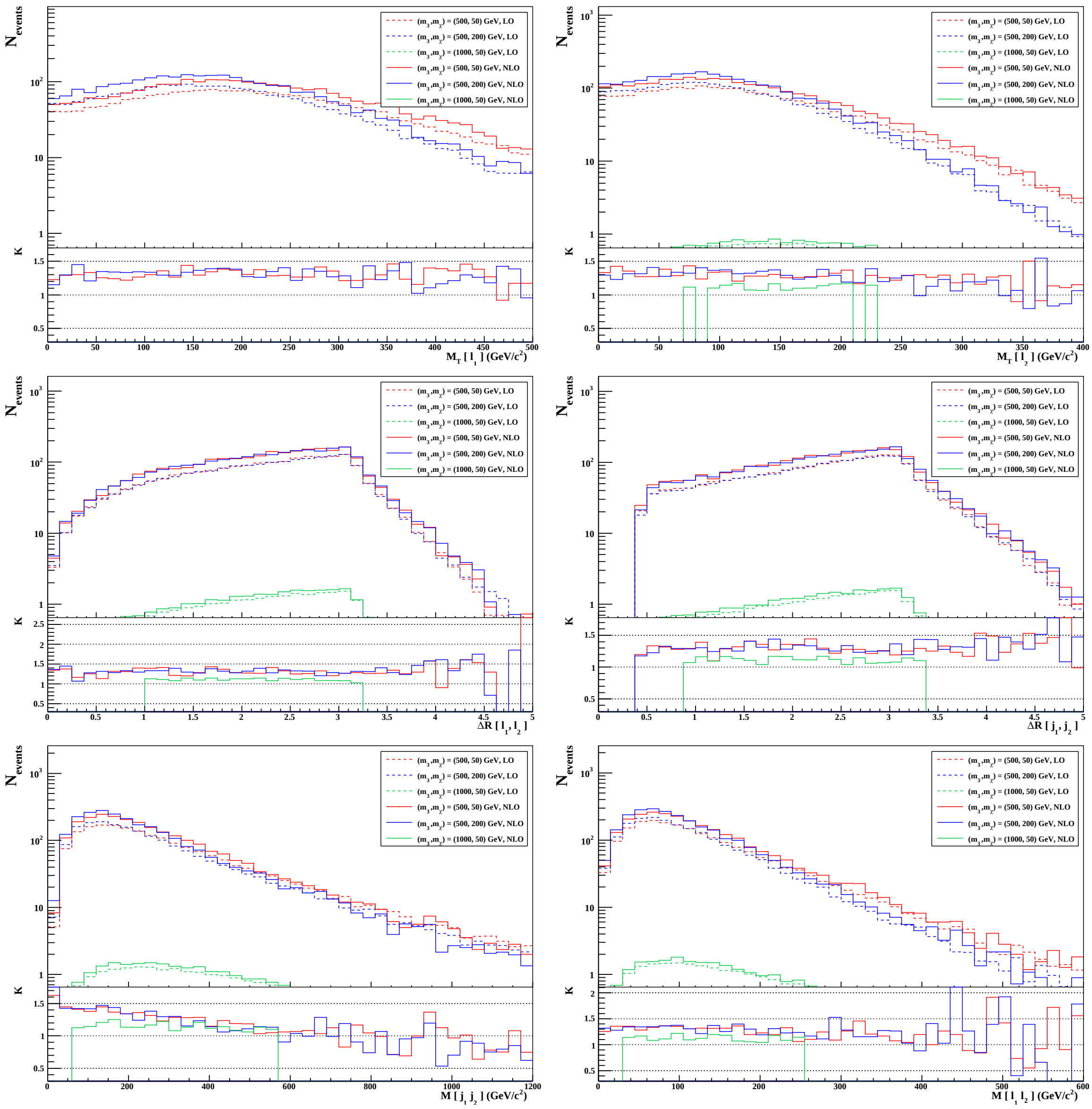

Figure 7: Dilepton signal region: jet and lepton properties (continued).

References

[1] J. Alwall, R. Frederix, S. Frixione, V. Hirschi, F. Maltoni, et al., *The automated computation of tree-level and next-to-leading order differential cross sections, and their matching to parton shower simulations*, *JHEP* **1407** (2014) 079, [`arXiv:1405.0301`].

[2] C. Degrande, C. Duhr, B. Fuks, D. Grellscheid, O. Mattelaer, et al., *UFO - The Universal FeynRules Output*, *Comput.Phys.Commun.* **183** (2012) 1201–1214, [`arXiv:1108.2040`].

[3] A. Alloul, N. D. Christensen, C. Degrande, C. Duhr, and B. Fuks, *FeynRules 2.0 - A complete toolbox for tree-level phenomenology*, *Comput.Phys.Commun.* **185** (2014) 2250–2300, [`arXiv:1310.1921`].

[4] C. Degrande, *Automatic evaluation of UV and R2 terms for beyond the Standard Model Lagrangians: a proof-of-principle*, `arXiv:1406.3030`.

[5] C. Degrande, B. Fuks, V. Hirschi, J. Proudom, and H.-S. Shao, *Automated next-to-leading order predictions for colored scalar production at the LHC*, `to appear`.

[6] P. Artoisenet, R. Frederix, O. Mattelaer, and R. Rietkerk, *Automatic spin-entangled decays of heavy resonances in Monte Carlo simulations*, *JHEP* **1303** (2013) 015, [`arXiv:1212.3460`].

[7] T. Sjostrand, S. Mrenna, and P. Z. Skands, *A Brief Introduction to PYTHIA 8.1*, *Comput.Phys.Commun.* **178** (2008) 852–867, [`arXiv:0710.3820`].

[8] M. Cacciari, G. P. Salam, and G. Soyez, *The Anti-k(t) Jet Clustering Algorithm*, *JHEP* **0804** (2008) 063.

[9] M. Cacciari, G. P. Salam, and G. Soyez, *FastJet User Manual*, *Eur.Phys.J.* **C72** (2012) 1896.

[10] E. Conte, B. Fuks, and G. Serret, *MadAnalysis 5, A User-Friendly Framework for Collider Phenomenology*, *Comput.Phys.Commun.* **184** (2013) 222–256, [`arXiv:1206.1599`].